

Article

# Investigating Microstructural and Mechanical Behavior of DLP-Printed Nickel Microparticle Composites

Benny Susanto <sup>1,†</sup>, Vishnu Vijay Kumar <sup>2,†</sup>, Leonard Sean <sup>3,†</sup> , Murni Handayani <sup>4</sup> , Farid Triawan <sup>5</sup> ,  
Yosephin Dewiani Rahmayanti <sup>4</sup> , Haris Ardianto <sup>3,6</sup>  and Muhammad Akhsin Muflikhun <sup>3,\*</sup> 

- <sup>1</sup> PLN Puslitbang, Jl. Duren Tiga Raya No.102, Pancoran, Kota Jakarta Selatan, Jakarta 12760, Indonesia  
<sup>2</sup> International Institute of Aerospace Engineering and Management, Jain Deemed-to-be-University, JGI Global Campus, Bangalore 562112, India  
<sup>3</sup> Department of Mechanical and Industrial Engineering, Universitas Gadjah Mada, Jl. Grafika No. 2, Yogyakarta 55281, Indonesia  
<sup>4</sup> Research Center for Nanotechnology Systems, National Research and Innovation Agency (BRIN), Puspptek Area, Tangerang Selatan 15314, Indonesia  
<sup>5</sup> Department of Mechanical Engineering, Sampoerna University, Jl. Raya Pasar Minggu No.Kav. 16, Kec. Pancoran, Jakarta 12780, Indonesia  
<sup>6</sup> Department of Aerospace Engineering, Sekolah Tinggi Teknologi Kedirgantaraan, Jl. Parangtritis km. 4,5, Yogyakarta 55281, Indonesia  
\* Correspondence: akhsin.muflikhun@ugm.ac.id  
† These authors contributed equally to this work.

**Abstract:** The study investigates the fabrication and analysis of nickel microparticle-reinforced composites fabricated using the digital light processing (DLP) technique. A slurry is prepared by incorporating Ni-micro particles into a resin vat; it is thoroughly mixed to achieve homogeneity. Turbidity fluctuations are observed, initially peaking at 50% within the first two minutes of mixing and then stabilizing at 30% after 15–60 min. FTIR spectroscopy with varying Ni wt.% is performed to study the alterations in the composite material's molecular structure and bonding environment. Spectrophotometric analysis revealed distinctive transmittance signatures at specific wavelengths, particularly within the visible light spectrum, with a notable peak at 532 nm. The effects of printing orientation in the X, Y, and Z axes were also studied. Mechanical properties were computed using tensile strength, surface roughness, and hardness. The results indicate substantial enhancements in the tensile properties, with notable increases of 75.5% in the ultimate tensile strength and 160% in the maximum strain. Minimal alterations in surface roughness and hardness suggest favorable printability. Microscopic examination revealed characteristic fracture patterns in the particulate composite at different values for the wt.% of nickel. The findings demonstrate the potential of DLP-fabricated Ni-reinforced composites for applications demanding enhanced mechanical performance while maintaining favorable printability, paving the way for further exploration in this domain.

**Keywords:** particulate composites; additive manufacturing; nickel microparticles; digital light processing



**Citation:** Susanto, B.; Kumar, V.V.; Sean, L.; Handayani, M.; Triawan, F.; Rahmayanti, Y.D.; Ardianto, H.; Muflikhun, M.A. Investigating Microstructural and Mechanical Behavior of DLP-Printed Nickel Microparticle Composites. *J. Compos. Sci.* **2024**, *8*, 247. <https://doi.org/10.3390/jcs8070247>

Academic Editor: Francesco Tornabene

Received: 30 April 2024

Revised: 25 May 2024

Accepted: 28 May 2024

Published: 29 June 2024



**Copyright:** © 2024 by the authors. Licensee MDPI, Basel, Switzerland. This article is an open access article distributed under the terms and conditions of the Creative Commons Attribution (CC BY) license (<https://creativecommons.org/licenses/by/4.0/>).

## 1. Introduction

Composite materials are used in every field of engineering, like aerospace, construction, communication, military, ocean structure, and various other high-performance applications, owing to their high specific strength and modulus, increased design flexibility, desirable thermal expansion characteristics, good resistance to fatigue and corrosion, and economic efficiency [1–3]. Additive manufacturing (AM) has redefined the design process and the manufacturing of materials, components, and products in different sectors [4,5]. Among the many AM processes, digital light processing (DLP) printing has attracted significant interest, as it is capable of generating complex geometries with high accuracy and resolution. AM technology using photosensitive resin was first developed to cure resins

using a precisely controlled laser involving DLP. Studies have shown that it is possible to develop a method for printing large models using a small DLP printer [6]. Introducing microparticles during AM processes is an important area for research because of the possibility of numerous property improvements such as mechanical, chemical, electrical, biological, and thermal characteristics of the printed components [7–9]. Though the introduction of microparticles has shown improvements in properties, the refractive index of the printing material strongly influences the curability and curing time of the printing photopolymers.

Micro- and nanoparticle-incorporated composites have shown superior properties [10,11]. A study on incorporating silicon nanoparticles like SiO<sub>2</sub>, montmorillonite, and attapulgite found that printing was impossible with more than 10% filler concentration [12]. Nanographite dispersion with stereolithography has shown improvement in properties in the resulting composite [13]. The dispersion of nanoparticles in the base matrix is critical for maintaining homogeneous material characteristics. Agglomeration and sedimentation may occur if the nanoparticle surfaces do not adhere properly to the base matrix [14]. Nickel microparticles are widely employed in various applications due to their unique features, which include high strength, great corrosion resistance, and strong thermal conductivity. Adding nickel (Ni) microparticles to composite materials can improve their mechanical and functional performance. Adding a small quantity of Ni to iron can produce a corrosion-resistant Ni-based stainless steel [15]. Ni is used as a surface coating in electroplating to avoid substrate corrosion [16]. Ni plating has shown excellent biofouling reduction in seawater [17]. In recent years, the lithium battery industry has been inextricably linked with Ni; adding Ni to the battery can boost energy density while simultaneously lowering costs [18]. However, the characteristics of nickel microparticle composite materials created with DLP printing have not been thoroughly investigated.

DLP printing has produced various materials, including polymers, ceramics, and metals. A study on incorporating silver nanoparticles was performed with 3D conductive structures created by integrating silver nitrate into a photocurable oligomer in the presence of appropriate photoinitiators and subjecting them to a digital light system [19]. DLP-based manufacturing of zirconia scaffolds with 2–20% hydroxyapatite composites showed comparable mechanical strength and good cell proliferation and differentiation [20]. DLP-printed nanocomposite samples were reinforced with copper and magnetite nanoparticles and carbon nanofibers aligning and condensing conductive nanoparticles to produce embedded electronic components [21]. DLP printing incorporating metal microparticles remains an area of limited exploration, with only a few studies on this topic.

While some studies have explored the use of metal microparticles with DLP, the application of nickel microparticles as composite materials in DLP printing is still in its early stages. This study investigates the properties of nickel microparticle-reinforced composites fabricated using digital light processing (DLP). The results of this study provide insights into the possible uses of nickel microparticle composite materials created using DLP printing, as well as help develop novel materials for various sectors.

## 2. Materials and Methods

A photopolymer ANYCUBIC-plant-based UV resin procured from Indonesia was employed for DLP printing using a DLP ANYCUBIC Photon Ultra Printer. The properties of the resin are listed in Table A1 and the specification of the 3D printer is given in Table A2, both in the Appendix section. The nickel microparticle size varies from 5–60 μm, as observed through a digital microscope, as depicted in Figure 1. The printing parameters are given in Table 1. Initially, the resin mixture with nickel powder was prepared by combining 200 mL of resin with the requisite weight percentage in a beaker using a digital Taffware scale. Stirring was conducted with an IKA RW 20 mechanical stirrer at 288 RPM for five minutes to prevent gas bubble formation.

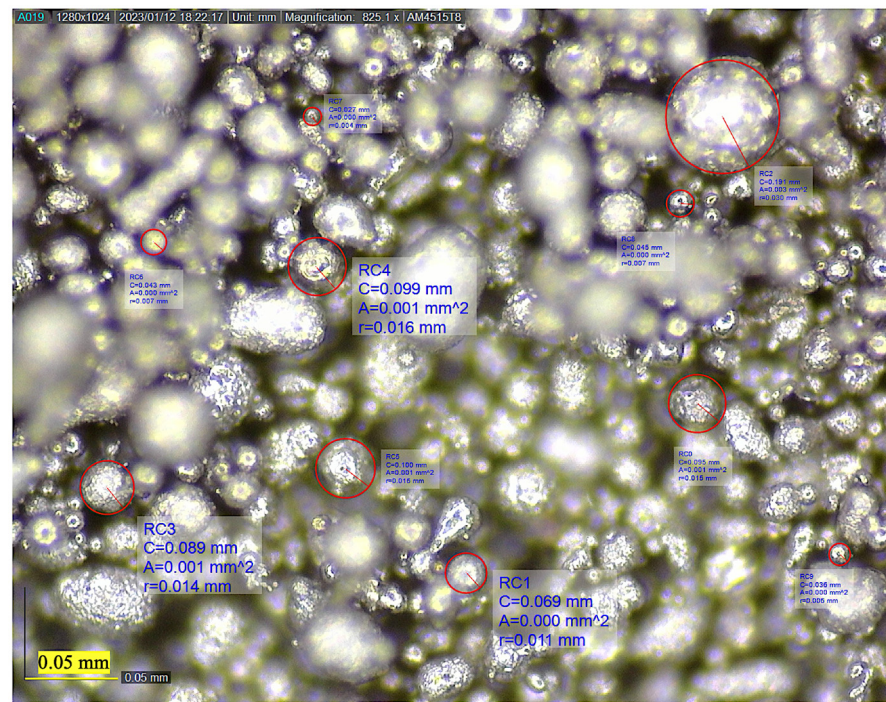


Figure 1. Digital microscope image showing the structure and morphology of the nickel microparticles.

Table 1. Printing parameters.

| Printing Parameters     | Values | Unit   |
|-------------------------|--------|--------|
| Exposure time           | 2      | s      |
| Lifting platform height | 5      | mm     |
| Lifting speed           | 120    | mm/min |
| Bottom exposure time    | 35     | s      |
| Layer height            | 0.05   | mm     |
| Retracting speed        | 120    | mm/min |

The turbidity absorbance was plotted on a mixture of uncured micro-nickel resin with the mixing ratio that demonstrated the highest tensile characteristics while guaranteeing complete mixing. The material was scanned between 320–1100 nm at 0, 2, 4, 6, 8, 10, 15, 20, 25, 30, 40, 50, and 60 min. The results were then compared to those of a solution containing only photoretin. The mixture was then poured into the 3D DLP resin machine reservoir for printing. Subsequently, .stl format files were executed on the DLP printer, with the printing duration determined by the specimen’s height along the z-axis. The printed specimens were rinsed in an alcohol solution, followed by curing for 24 h under ambient conditions. The testing involves determining the orientation of the tensile specimen, as categorized into horizontal and vertical printing, as shown in Figure 2.

Tests were conducted under two conditions: without additional particles (0 wt.%) and with 1 wt.% nickel microparticles. Orientation is considered optimal if it exhibits high tensile strength, maximum tensile load, high break elongation, and high break strain, while being generally repeatable. The research methodology is depicted in Figure A1 in Appendix A. The turbidity assessment is performed through spectrophotometric analysis of diverse values of wt.% of nickel microparticles integrated within the resin. FTIR spectroscopy of the resin samples with various nickel concentrations, ranging from 0 wt.% to 8 wt.%, and composed of Ni microparticles, are analyzed. The morphology and chemical composition of the specimens were characterized using various analytical techniques. Prior to analysis, the samples were sputter-coated with a thin film of gold to render them conductive for electron microscopy. Thermo-scientific equipment for scanning electron microscopy (SEM) was

employed to examine the surface topography and microstructural features of the specimens. Energy dispersive X-ray spectroscopy (EDS) was performed in conjunction with SEM to obtain localized elemental compositions at the interface regions and neighboring areas. EDS mapping enabled the visualization of the spatial distribution of different elements within the samples, facilitating a comprehensive understanding of their elemental makeup and identifying the specific materials present at various locations.

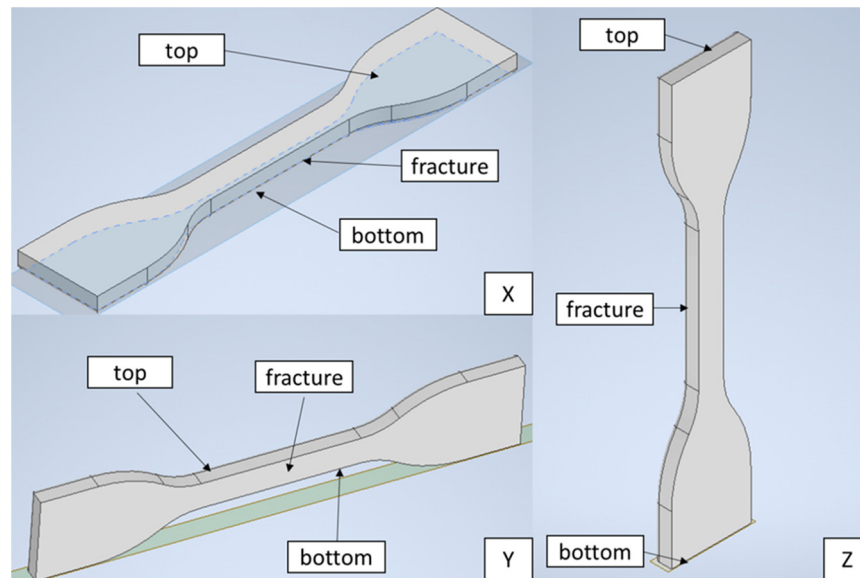


**Figure 2.** Schematic representation of different printing orientations of the tensile testing specimens: X, Y, and Z.

This study investigates the optimal printing orientation for 3D parts and the ideal nickel wt.% for enhanced performance. The investigation also evaluates the mechanical characteristics of various samples, including tensile strength, surface roughness, and material hardness, as a function of the increasing nickel content in the specimens. Microscopic observations elucidate the failure mechanisms occurring in the composite. The test results we obtained are examined and compared with findings in the literature to reach meaningful conclusions. A dedicated model is employed for conducting surface roughness with standard ISO 2021 [22] Shore D hardness, as per standard ASTM D2240-15 [23], and tensile testing as per ASTM D638 [23] type IV standard. Once the orientation is selected, the investigation determines the appropriate nickel ratio in the particle composite. Tensile tests were performed on photoreins with various nickel mass ratios, ranging from 2% to 8%. The collected data were evaluated to identify the optimal nickel wt.% ratio, which exhibits superior mechanical characteristics, including high tensile strength and maximum tensile load, break elongation, and break strain. The samples were then inspected using an AM4515T8 Dino-lite Edge DINOLITE digital microscope, Taiwan.

### 3. Results and Discussion

#### 3.1. Spectrophotometric Analysis

Spectrophotometric analysis revealed distinctive transmittance signatures at specific wavelengths, particularly within the visible light spectrum, with a notable peak at 532 nm for all samples except the control, as shown in Figure 3a. This characteristic absorption pattern indicates the unique properties of the resin, which fully absorbs most of the UV light (324–444 nm) and visible light (660–694 nm) associated with the green color of the photorein. The absorbance spectrum, which is complementary to the transmittance spectrum, provides information about the ability of the resin–micro-Ni mixture to absorb light at different wavelengths. The presence of nickel microparticles initially resulted in high absorbance across the spectrum, as shown in Figure 3b. The analysis further revealed a

time-dependent trend in the transmittance and absorbance of the resin–nickel micropowder solution, as represented in Figure 3c.

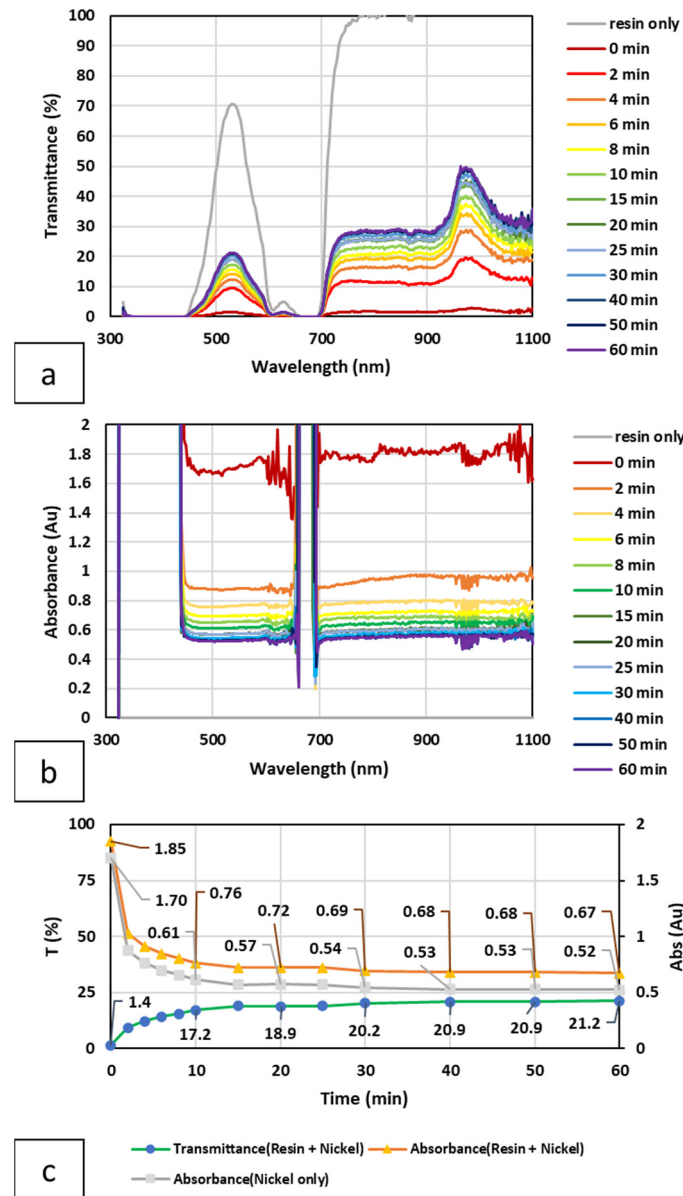


**Figure 3.** UV-Vis spectrophotometry analysis of the resin–micro-Ni mixture showing (a) transmittance spectrum; (b) absorbance spectrum; and (c) transmission and absorbance of the mixture in the wavelength of 532 nm as a factor of time.

Initially, the presence of nickel microparticles results in high absorbance across the spectrum, gradually transitioning to higher transmittance over time, and corresponding to a decrease in absorbance. The literature suggests a linear correlation between turbidity and absorbance, particularly at a wavelength peak of 532 nm. Examination of the absorbance solely attributed to nickel microparticles revealed a rapid reduction in light absorbance within the initial 2 min, followed by stabilization between 15 and 60 min. This indicates a turbidity reduction of approximately 50% within the first 2 min, stabilizing at approximately 30% thereafter. Previous research highlights the rapid sedimentation of resin–microparticle mixtures, with nanosized particles demonstrating superior suspension stability compared to microparticles [24]. Nonetheless, microparticle suspension stability can still be achieved within a shorter timeframe, typically under 12 h. Interestingly, the observed decrease in

light absorbance over time may imply the presence of self-cleaning capabilities in the resin–nickel micropowder composite. As the microparticles settle, the resin surface becomes more transparent, possibly improving the material’s capacity to collect and use light energy for a variety of purposes. Further research into the long-term stability and optical performance of this composite system might yield useful insights into its practical uses. Nevertheless, microparticle suspension stability may be attained in a shorter timescale, usually less than 12 h.

### 3.2. Fourier Transform Infrared (FT-IR) Spectroscopy

The spectral analysis provides insights into the chemical structure and composition variations resulting from the incorporation of nickel microparticles into the resin matrix. Figure 4 depicts the FT-IR spectra of the resin samples with various nickel concentrations ranging from 0 wt.% to 8 wt.%. The FT-IR spectrum of the resin without nickel exhibited distinct peaks at 1722, 1637, and 1110  $\text{cm}^{-1}$ , corresponding to C=O, C=C, and C=O bonds, respectively. Upon adding 1, 2, and 4 wt.% nickel, the resin–Ni micro composites displayed similar peaks at 2360, 1670, and 1558  $\text{cm}^{-1}$ , indicating consistent chemical compositions. Specifically, the peak at 2360  $\text{cm}^{-1}$  is associated with C $\equiv$ N, while the bands at 1670 and 1558  $\text{cm}^{-1}$  correspond to C=C and C=N bonds, respectively. Conversely, resin–Ni micro composites containing 6 and 8 wt.% nickel exhibited additional peaks at 1724 and 1647  $\text{cm}^{-1}$ , attributed to C=O and C=C/C=N bonds, respectively, in addition to the characteristic peaks observed in the lower nickel concentration composites. This suggests that the higher concentrations of nickel induce more significant changes in the chemical bonding and molecular structure of the resin. The inference from the FT-IR study suggested that the addition of nickel microparticles to the resin affects the chemical composition, resulting in changes in the FT-IR spectra. New peaks develop, and peak locations vary, indicating changes in the composite material’s molecular structure and bonding environment. This information is critical for understanding how the resin matrix interacts with nickel particles, which can affect the composite material’s overall characteristics and performance.

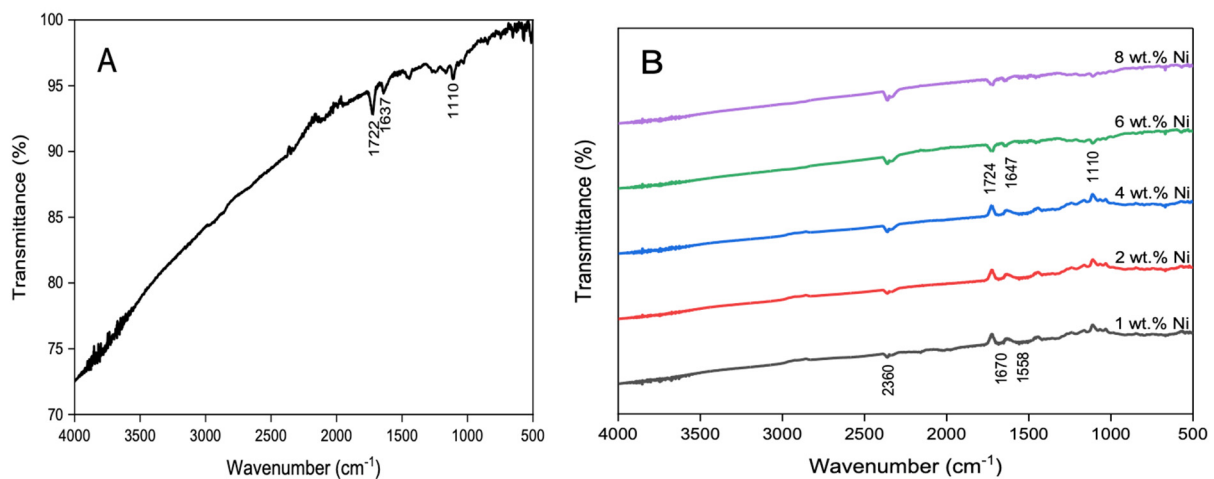


**Figure 4.** FT-IR spectra of 0 wt.% Ni (A) and (B) resin–Ni micro composites with different Ni wt.%.

### 3.3. Tensile Testing

Figure 5 depicts the various specimens after tensile testing. Figure 6 shows the stress–strain curve for the composites with different Ni wt.%. The composite containing 6 wt.% nickel has the capacity to endure the highest maximum load, along with the highest maximum tensile stress, elongation, and strain. The control sample registers the lowest values, followed by notable increases in the 1% and 2% nickel mass fractions. Within the 4% nickel mass fraction mixture, enhancements in the mechanical properties are discernible solely in the maximum load and maximum tensile stress thresholds. Finally, as compared to the 6% counterpart, the 8% nickel mass fraction combination has a greater

mechanical characteristic. This trend is consistent with the findings that have reported that the mechanical performance of polymer composites reinforced with ceramic microparticles often determines an optimal filler content, beyond which the properties start to decline due to agglomeration and poor particle dispersion [24,25].

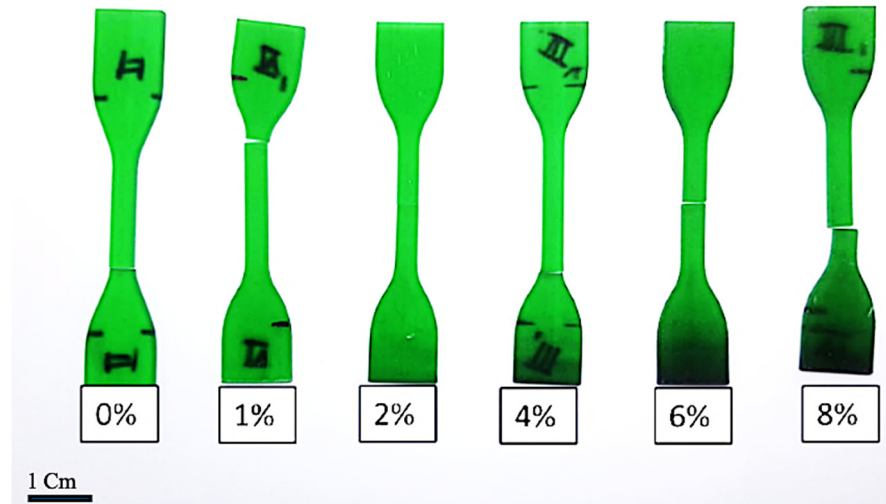


Figure 5. Tensile specimens post-testing.

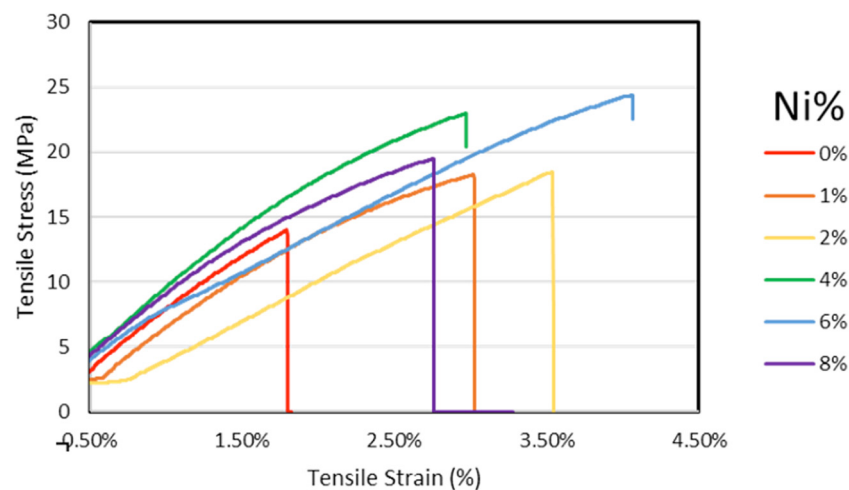
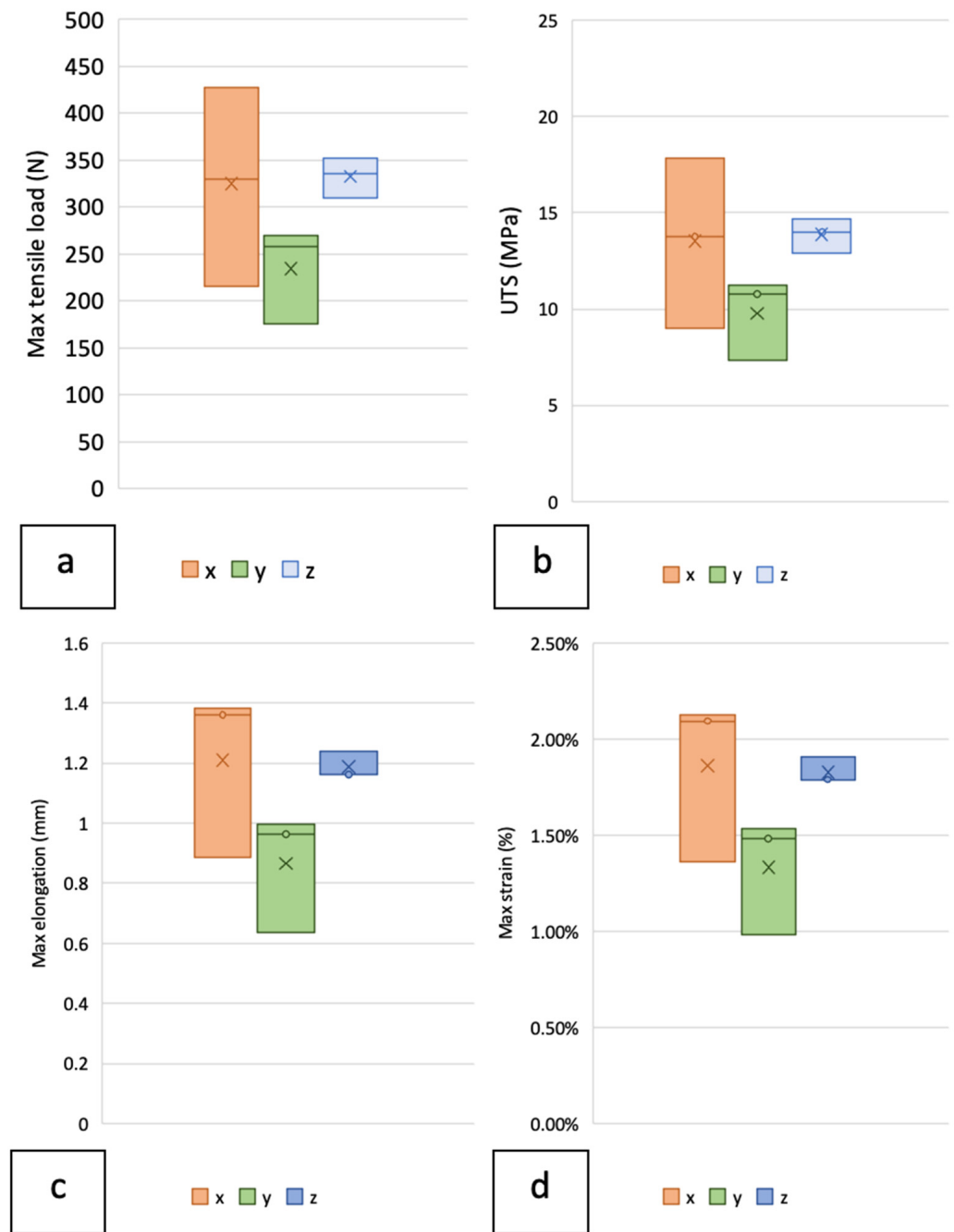


Figure 6. Stress–strain curves from tensile testing of the resin–Ni composites with different Ni wt.%.

The test outcomes were evaluated for three distinct orientations, namely, X, Y, and Z, each with a mass fraction of 0%, as depicted in Figure 7; the orientations follow the configuration shown in Figure 2. These orientations exhibited varying maximum tensile loads, ultimate tensile strengths, break elongations, and break strains. Specimen X demonstrated the highest tensile properties across all parameters, albeit with a noticeable deviation along the X-axis compared to the Z orientation. Conversely, the Y orientation displayed the lowest load-bearing capacity and tensile strength among the three orientations. Notably, the X orientation proved to be the most effective, yielding relatively high values of tensile properties while maintaining repeatability. Further testing with 1 wt.% nickel confirmed the superiority of printing in the Z orientation, as illustrated in Figure 8. The Z orientation exhibited the highest values across all the tested mechanical parameters, with minimal deviations [26,27].



**Figure 7.** (a) Maximum tensile load, (b) ultimate tensile strength (UTS), (c) maximum elongation, and (d) maximum strain of tensile specimens with 0% weight nickel (Ni) across orientations X, Y, and Z.

From the findings above, it is evident that printing in the Z orientation offers superior results compared to printing in either the X or the Y orientation. As a result, further printing with a higher nickel wt.% exclusively occurred in the Z orientation. Tensile tests were then conducted on specimens with varying nickel mass ratios in the photoresin, including 2%, 4%, 6%, and 8%. The collected data include mechanical properties such as maximum tensile load, ultimate tensile stress, break elongation, and break strain. The results of these tensile tests are illustrated in Figure 9. The graph shows a gradual increase in maximum tensile load and ultimate tensile strength, with an increasing mass fraction of nickel within the composite material. As the nickel mass fraction increases to 1%, 2%, and 4%, there is a consistent increase in both the maximum load and tensile strength. However, the alterations in elongation and strain remain relatively marginal. At a 6%

nickel mass fraction, a conspicuous peak emerges in both the maximum load (568 N) and tensile strength (23.7 MPa), coinciding with a peak in elongation and strain, indicating optimal material performance (1.88 mm, 2.89%). Intriguingly, when the nickel mass fraction increased to 8%, a notable decrease was observed in the maximum load (457 N), tensile strength (18.8 MPa), elongation (1.74 mm), and strain (2.68%) compared to those of the 6% nickel fraction, signifying a less favorable performance.

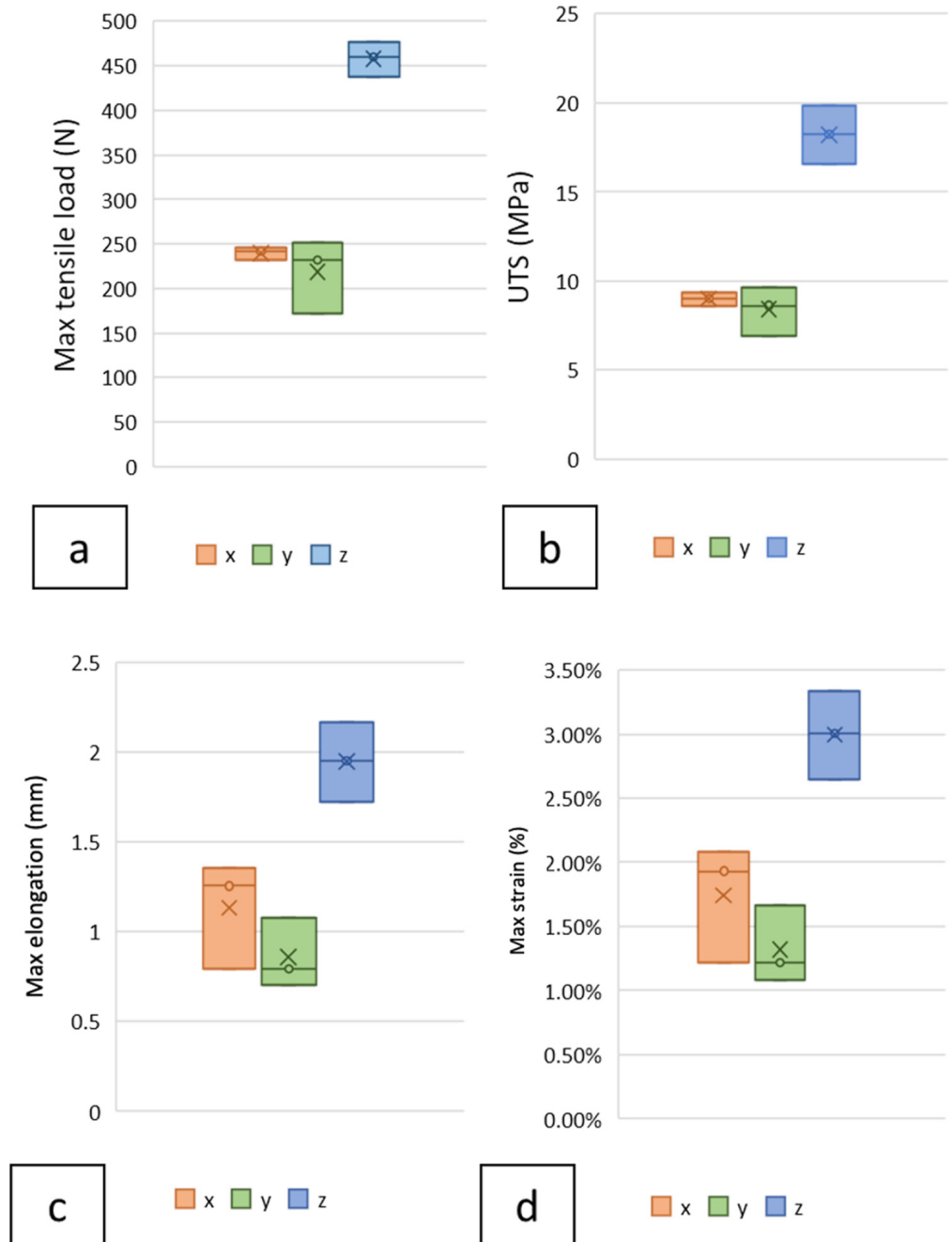


**Figure 8.** (a) Maximum tensile load, (b) ultimate tensile strength (UTS), (c) maximum elongation, and (d) maximum strain of tensile specimens with 1% weight nickel (Ni) across orientations X, Y, and Z.

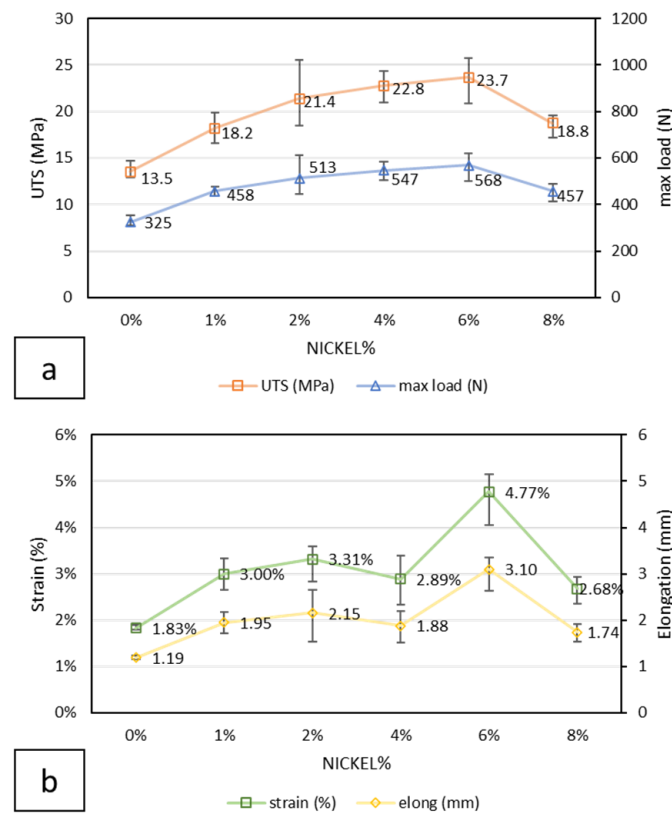


**Figure 9.** The progression of the mechanical characteristics of the resin–Ni micro composite compared to those of the Ni wt.% composite: (a) maximum tensile load and UTS; (b) maximum elongation and maximum strain.

### 3.4. Surface Roughness and Hardness

Surface roughness assessments revealed a notable increase in surface roughness following a 6% increase in the Ni content, as shown in Figure 10a. The hardness measurements exhibit marginal deviations in the Shore D values with increasing Ni wt.%, as depicted in Figure 10b. The marginal deviations in the hardness measurements with increasing Ni wt.% suggest that the DLP 3D printer can maintain a consistent printing precision despite the addition of metal particles. This is consistent with the findings of other studies, which have reported the high precision and accuracy of DLP 3D printers for composite material printing [28,29]. Similarly, a study reported that the surface roughness of a composite material increased with the addition of ceramic particles, which affected the printing quality and accuracy [30].

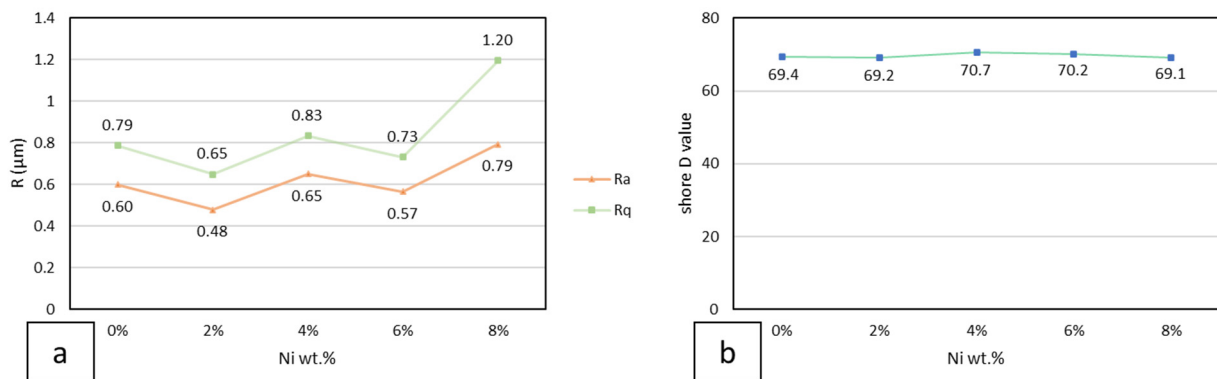


**Figure 10.** (a) Surface roughness and (b) shore hardness of samples with different Ni contents.

### 3.5. Microstructures and Fracture Mechanism

The observational findings from the printing orientations X and Y reveal a coarse texture in both the initial and final layers, closely resembling the printing surfaces, as outlined in Figure 11.

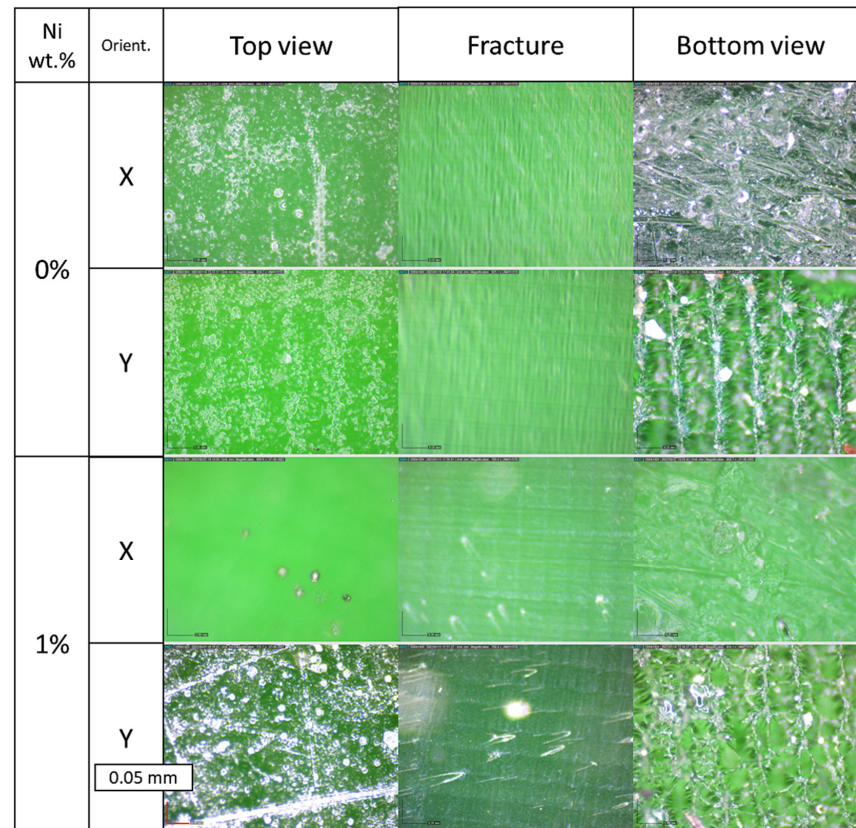


**Figure 11.** Microstructure of the resin–micro-Ni composite in the X- and Y-printed orientations.

Notably, nickel microparticles are suspended in the X orientation. This suspension of nickel microparticles in the X orientation suggests a more homogeneous dispersion of the filler within the resin matrix compared to the Y orientation. Further examination of the fracture region in both the X- and Y-orientations revealed a distinct layer-by-layer printing pattern indicative of brittle fracture.

The presence of nickel microparticles suspended in the resin is indicated by the formation of crazing in the resin. This finding is consistent with earlier research on the fracture behavior of polymer-based composites, in which the layered structure produced during the additive manufacturing process might contribute to preferential crack propagation along the printing interface [31]. Similarly, in both the X and Y orientations, the development of cavities on the top and bottom layers intensifies with nickel microparticles in the printed specimens in the Z orientation. Moreover, there is a gradual increase in the size and volume of the crazing observed in the fracture region, as outlined in Figure 12. The lack of nickel microparticles in the fracture area indicates a weakened bond between the particles and the matrix.

The micrographs in Figures 11 and 12 reveal a notable difference in the distribution of nickel (Ni) particles through the thickness of the additively manufactured composite samples. The bottom regions exhibit a higher concentration of dense Ni particles, compared to the top regions. This non-uniform particle distribution is likely attributable to particle settling effects during the printing process. Despite the relatively high viscosity of the photocurable resin used, the denser Ni particles may gradually sink and accumulate at the bottom of the resin–particle slurry prior to the curing of each layer. Alternatively, if

a bottom-up printing sequence were to be employed, the initial layers would inherently have higher particle loadings from the as-mixed slurry before settling occurred. This particle segregation can have significant impacts on the local and overall mechanical response of the printed composites. The particle-rich bottom regions can be expected to exhibit higher stiffness and strength due to the increased reinforcement from the higher Ni content acting as rigid constraints on the polymer matrix. However, these regions may also suffer from reduced ductility and toughness compared to the polymer-rich top layers. Additionally, the highly loaded bottom layers face an increased propensity for particle agglomeration, defect formation, and compromised interfacial integrity—acting as precursors to premature failure.

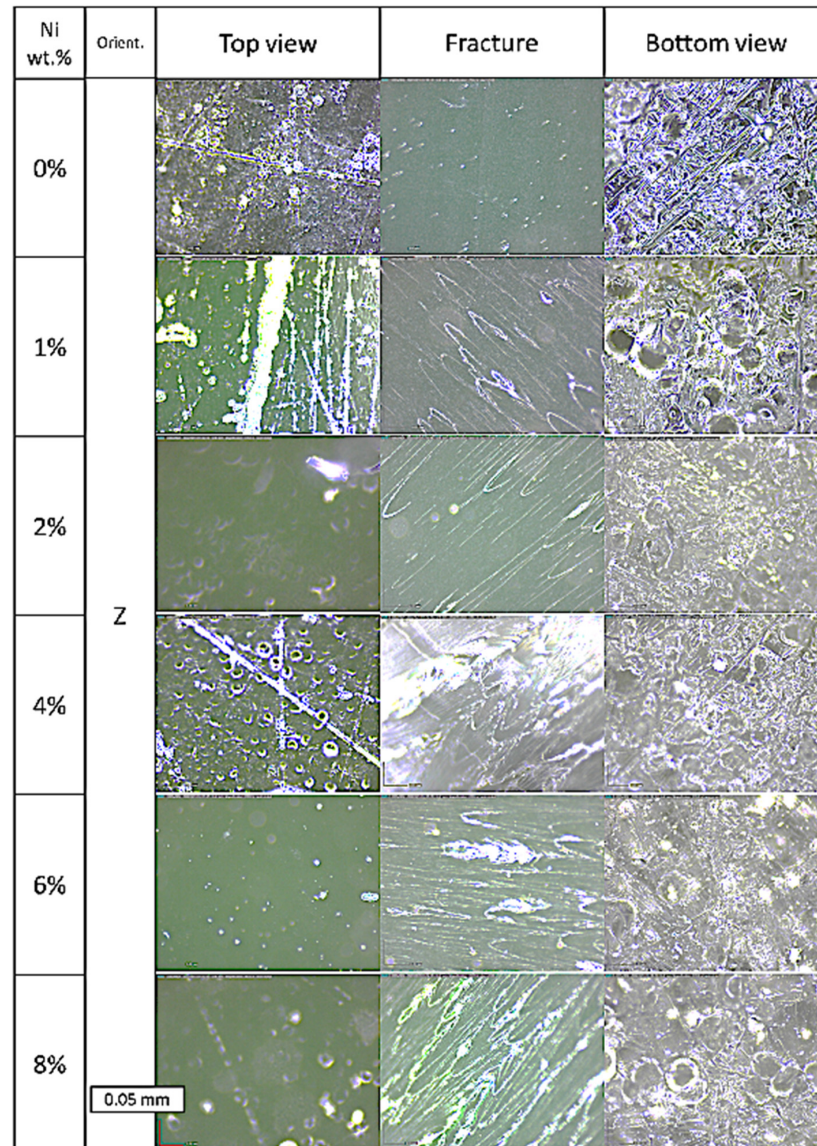


**Figure 12.** Microscopic structure of the resin–micro-Ni composite in the Z-printed orientation.

Figure 13 shows the SEM images of the plain resin composite and the resin–micro-Ni composite. The SEM images clearly show the successful incorporation of nickel (Ni) microparticles into the polymer resin matrix to form the resin–Ni composites. The Ni particles are well dispersed and embedded throughout the resin, indicating good interfacial bonding between the filler and matrix phases. It is well established that the content of the reinforcing filler phase plays a critical role in determining the mechanical performance of particulate-reinforced polymer composites. As the Ni particle loading increases, the composites can be

expected to exhibit higher stiffness and strength due to increased constraint of the polymer chains by the rigid Ni particles. However, too high of a filler content can lead to particle agglomeration, increased defect concentration, and poor interfacial adhesion—resulting in premature failure and loss of toughness. The SEM images revealed typical particulate composite fracture features, suggesting reasonably good particle–matrix bonding aided by the photocuring process. However, some non-uniform Ni dispersion was noted, which could be a precursor to interfacial damage evolution.

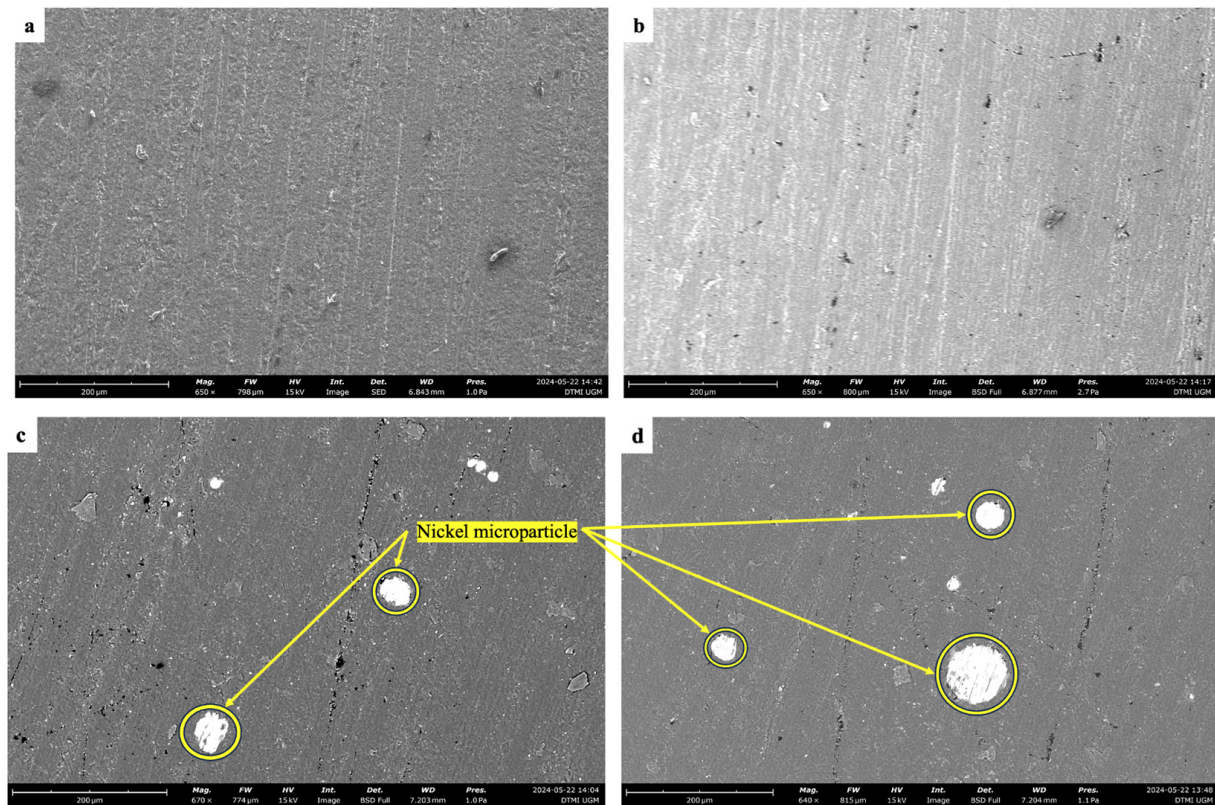


**Figure 13.** SEM images representing (a,b): resin composite, (c,d) resin–micro-Ni composite.

Figure 14a shows the plain resin with a uniform carbon and oxygen signal from the polymer matrix. For the resin–micro-Ni composite, Figure 14b reveals the interfacial regions where nickel particles are embedded within the carbon/oxygen-rich resin. The quality of this particle–matrix interface is crucial for mechanical integrity. The quality and characteristics of this particle–matrix interface play a pivotal role in dictating the efficiency of load transfer and determining the overall mechanical performance. Good interfacial bonding without defects or deleterious reactions is essential. Figure 14c depicts resin-rich areas containing isolated nickel particles, indicating some non-uniformity in the nickel dispersion. The presence of these individual nickel particles, rather than a continuous nickel phase, suggests that some level of non-uniformity or particle clustering occurred during the printing process. Such heterogeneities could serve as initiation sites for damage and premature failure. Finally, Figure 14d clearly distinguishes the dense nickel particulate reinforcement phase within the composite microstructure. The nickel particles appear dense and distinct, with well-defined morphologies and minimal interfacial phases or reactions evident. Preserving the intrinsic nature of the nickel particles is important for realizing their full reinforcing potential.

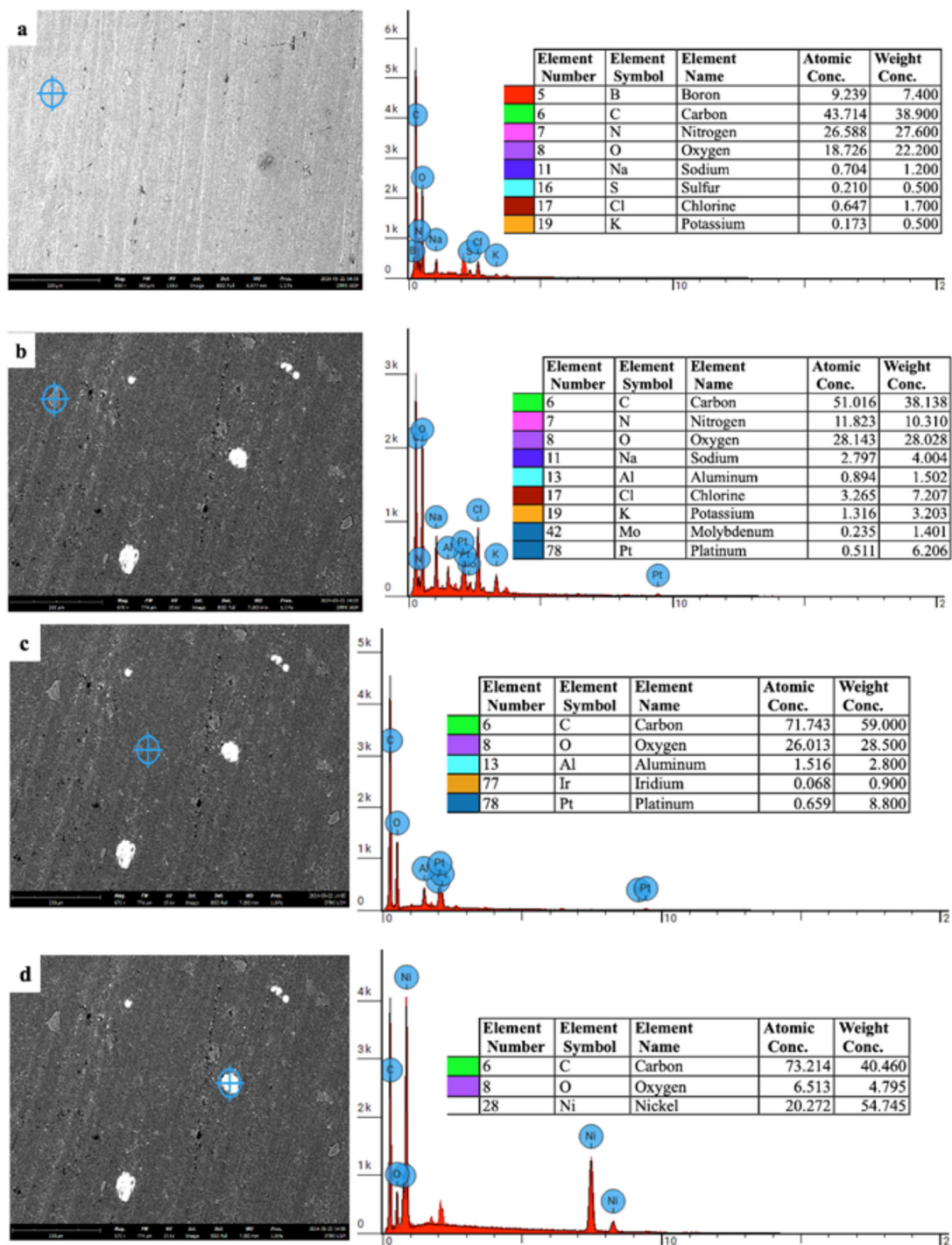


**Figure 14.** EDS images representing (a) resin composite, (b) interface region in resin-micro-Ni composite, (c) resin region in resin-micro-Ni composite, and (d) Ni in resin-micro-Ni composite.

The observed enhancements in tensile strength, elongation, and toughness with increasing Ni content up to 6 wt.% can be attributed to effective load transfer from the ductile resin matrix to the reinforcing Ni particles. The rigid Ni particles contribute to the constraint of the polymer chain mobility and plastic deformation processes. However, at higher Ni loadings above the optimum 6 wt.%, the formation of particle agglomerates and increased interfacial defects appears to degrade mechanical performance. In addition to filler content, the size of the Ni particles may also influence mechanical behavior. Smaller particle sizes provide more surface area for matrix-particle interactions and efficient load

transfer. Composites with finer Ni particles could, therefore, offer higher stiffness and strength compared to those with larger particles at the same filler loading. However, very fine particle sizes can also raise concerns, like increased particle agglomeration tendency.

#### 4. Conclusions

The research explores the effect of nickel microplastics on additively manufactured composite using the DLP technique. A mixture comprising 3D printing resin and nickel microparticles was prepared, with the concentration of nickel microparticles varying across different samples. The turbidity of the samples was analyzed, and the spectrophotometry test indicated a decrease in turbidity to approximately 50% within the first two minutes after the resin–nickel microparticle slurry was created. However, the slurry remains under stable conditions of 30% turbidity from 15 min to 60 min after mixing. The FT-IR spectrum of the resin without nickel exhibited distinct peaks at 1722, 1637, and 1110  $\text{cm}^{-1}$ , corresponding to C=O, C=C, and C=O bonds, respectively. Upon adding 1, 2, and 4 wt.% nickel, the resin–Ni micro composites displayed similar peaks at 2360, 1670, and 1558  $\text{cm}^{-1}$ , indicating consistent chemical compositions. The results from the tensile tests showed that the increase in the amount of nickel microparticles suspended in the resin translates to a peak in the mechanical characteristics at 6 wt.% nickel. The mechanical characteristics of the specimens increased slightly: the maximum tensile load was 568 N (74.7% increase), the UTS was 23.7 MPa (75.5% increase), the maximum elongation was 3.10 mm (160% increase), and the maximum strain was 4.77% (160% increase). Surface roughness assessments revealed a notable increase in surface roughness following a 6% increase in the Ni content. The hardness measurements exhibit marginal deviations in the Shore-D values with increasing Ni wt.%. Microscopic observation of the surfaces of the specimens revealed the fracture characteristics of a particulate composite but with uneven distributions of the nickel microparticles. The investigation demonstrated the considerable influence of changing nickel microparticle concentrations on the mechanical properties of the composite, with the best results reported at 6 wt.%. The study provides proper insights into the potential for incorporating nickel microparticles into the additive manufacturing of composite materials for various engineering applications.

**Author Contributions:** Conceptualization: M.A.M.; Methodology: B.S., V.V.K., L.S.; Investigation: B.S., L.S.; Validation: V.V.K., L.S.; Data curation: B.S., V.V.K., L.S.; Writing original draft—B.S., V.V.K., L.S., M.H., F.T., Y.D.R., H.A., M.A.M.; Writing- review and editing: B.S., V.V.K., M.A.M.; Supervision: M.A.M. All authors have read and agreed to the published version of the manuscript.

**Funding:** This research received funding from Hibah RIIM 2023–2024, Indonesia.

**Data Availability Statement:** The data supporting the findings of this study are available upon request.

**Acknowledgments:** All authors gratefully acknowledge the anonymous reviewers for their valuable comments, which have significantly contributed to improving the quality of the manuscript and shaping it into an excellent paper.

**Conflicts of Interest:** The authors declare no conflicts of interest.

## Appendix A

**Table A1.** Properties of the photopolymers used in the experiment.

| Material Properties   | Values  | Unit          |
|-----------------------|---------|---------------|
| Deformation temp      | 60 ± 5  | °C            |
| Vitrification temp    | 55 ± 5  | °C            |
| Maximum elongation    | 8–12    | %             |
| Activation wavelength | 355–410 | nm            |
| Viscosity             | 150–350 | MPa.s (25 °C) |
| Bending strength      | 40–50   | MPa           |
| Tensile strength      | 35–45   | MPa           |

**Table A2.** Specification of DLP ANYCUBIC Photon Ultra Printer.

| Machine Specifications | Values                         | Unit            |
|------------------------|--------------------------------|-----------------|
| Machine weight         | 4                              | kg              |
| Printing dimensions    | 165 × 102.4 × 57.6             | mm <sup>3</sup> |
| Light source           | DLP optical projector          | -               |
| Z-axis resolution      | 0.01                           | mm              |
| Layer resolution       | 0.01~0.15                      | mm              |
| Control panel          | 2.8                            | Inch            |
| Data input             | USB                            | -               |
| Machine dimensions     | 383 × 222 × 227                | mm <sup>3</sup> |
| Printing technology    | DLP (Digital Light Processing) | -               |
| Max printing speed     | 60                             | mm/h            |
| XY resolution          | 0.08                           | mm              |
| Project resolution     | 1280 × 720                     | -               |
| Power supply           | 12                             | W               |

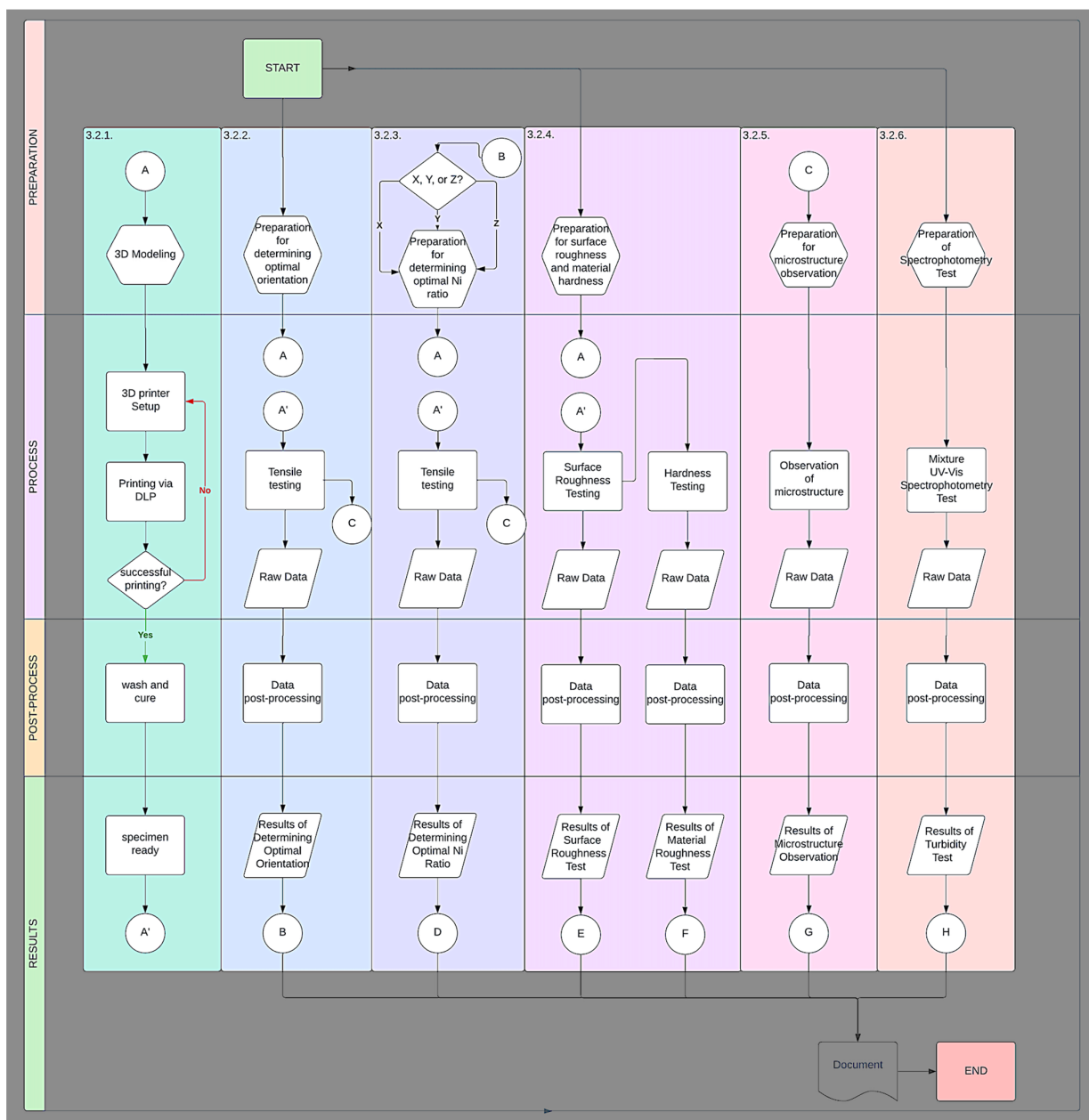


**Figure A1.** The flowchart diagram outlines the steps in manufacturing and testing.

## References

1. Tran, T.Q.; Lee, J.K.Y.; Chinnappan, A.; Jayathilaka, W.; Ji, D.; Kumar, V.V.; Ramakrishna, S. Strong, lightweight, and highly conductive CNT/Au/Cu wires from sputtering and electroplating methods. *J. Mater. Sci. Technol.* **2020**, *40*, 99–106. [\[CrossRef\]](#)
2. Kumar, V.V.; Balaganesan, G.; Lee, J.K.Y.; Neisiany, R.E.; Surendran, S.; Ramakrishna, S. A review of recent advances in nanoengineered polymer composites. *Polymers* **2019**, *11*, 644. [\[CrossRef\]](#) [\[PubMed\]](#)
3. Parveez, B.; Kittur, M.; Badruddin, I.A.; Kamangar, S.; Hussien, M.; Umarfarooq, M. Scientific advancements in composite materials for aircraft applications: A review. *Polymers* **2022**, *14*, 5007. [\[CrossRef\]](#) [\[PubMed\]](#)
4. Krajangsawasdi, N.; Blok, L.G.; Hamerton, I.; Longana, M.L.; Woods, B.K.S.; Ivanov, D.S. Fused deposition modelling of fibre reinforced polymer composites: A parametric review. *J. Compos. Sci.* **2021**, *5*, 29. [\[CrossRef\]](#)
5. Cai, H.; Chen, Y. A Review of Print Heads for Fused Filament Fabrication of Continuous Carbon Fiber-Reinforced Composites. *Micromachines* **2024**, *15*, 432. [\[CrossRef\]](#) [\[PubMed\]](#)
6. Wu, C.; Yi, R.; Liu, Y.J.; He, Y.; Wang, C.C. Delta DLP 3D printing with large size. In Proceedings of the 2016 IEEE/RSJ International Conference on Intelligent Robots and Systems (IROS), Daejeon, Republic of Korea, 9–14 October 2016; IEEE: Piscataway, NJ, USA, 2016.
7. Petousis, M.; Michailidis, N.; Papadakis, V.; Mountakis, N.; Argyros, A.; Spiridaki, M.; Moutsopoulou, A.; Nasikas, N.K.; Vidakis, N. The impact of the glass microparticles features on the engineering response of isotactic polypropylene in material extrusion 3D printing. *Mater. Today Commun.* **2023**, *37*, 107204. [\[CrossRef\]](#)
8. Iyyadurai, J.; Arockiasamy, F.S.; Manickam, T.S.; Suyambulingam, I.; Siengchin, S.; Appadurai, M.; Raj, E.F.I. Revolutionizing polymer composites: Boosting mechanical strength, thermal stability, water resistance, and sound absorption of cissus quadrangularis stem fibers with nano silica. *Silicon* **2023**, *15*, 6407–6419. [\[CrossRef\]](#)
9. Yuan, S.; Shen, F.; Chua, C.K.; Zhou, K. Polymeric composites for powder-based additive manufacturing: Materials and applications. *Prog. Polym. Sci.* **2019**, *91*, 141–168. [\[CrossRef\]](#)
10. Aryaswara, L.G.; Kusni, M.; Wijanarko, D.; Muflikhun, M.A. Advanced properties and failure characteristics of hybrid GFRP-matrix thin laminates modified by micro glass powder filler for hard structure applications. *J. Eng. Res.* **2023**, *in press*. [\[CrossRef\]](#)
11. Vijayan, M.; Selladurai, V.; Vijay Kumar, V.; Balaganesan, G.; Marimuthu, K. Low-Velocity Impact Response of Nano-Silica Reinforced Aluminum/PU/GFRP Laminates. In *International Symposium on Plasticity and Impact Mechanics*; Springer: Berlin/Heidelberg, Germany, 2022.
12. Weng, Z.; Zhou, Y.; Lin, W.; Senthil, T.; Wu, L. Structure-property relationship of nano enhanced stereolithography resin for desktop SLA 3D printer. *Compos. Part A Appl. Sci. Manuf.* **2016**, *88*, 234–242. [\[CrossRef\]](#)
13. Nugraha, A.D.; Kumar, V.V.; Gautama, J.P.; Wiranata, A.; Mangunkusumo, K.G.H.; Rasyid, M.I.; Dzanzani, R.; Muflikhun, M.A. Investigating the Characteristics of Nano-Graphite Composites Additively Manufactured Using Stereolithography. *Polymers* **2024**, *16*, 1021. [\[CrossRef\]](#)
14. Ramesh, M.; Niranjana, K.; Selvan, M.T. Wear and Friction Behavior of Biocomposites Fabricated Through Additive Manufacturing. In *Tribological Properties, Performance and Applications of Biocomposites*; John Wiley & Sons: Hoboken, NJ, USA, 2024; pp. 219–246.
15. Ha, H.-Y.; Lee, T.-H.; Kim, S.-D.; Jang, J.H.; Moon, J. Improvement of the corrosion resistance by addition of Ni in lean duplex stainless steels. *Metals* **2020**, *10*, 891. [\[CrossRef\]](#)
16. Huang, Y.; Zeng, X.T.; Hu, X.F.; Liu, F.M. Corrosion resistance properties of electroless nickel composite coatings. *Electrochim. Acta* **2004**, *49*, 4313–4319. [\[CrossRef\]](#)
17. Yang, D.; Lei, Y.; Xie, J.; Shu, Z.; Zheng, X. The microbial corrosion behaviour of Ni-P plating by sulfate-reducing bacteria biofouling in seawater. *Mater. Technol.* **2019**, *34*, 444–454. [\[CrossRef\]](#)
18. Feng, Y.; Yang, H.; Yang, Z.; Hu, C.; Wu, C.; Wu, L. A review of the design, properties, applications, and prospects of Ni-based composite powders. *Mater. Des.* **2021**, *208*, 109945. [\[CrossRef\]](#)
19. Fantino, E.; Chiappone, A.; Roppolo, I.; Manfredi, D.; Bongiovanni, R.; Pirri, C.F.; Calignano, F. 3D Printing of Conductive Complex Structures with In Situ Generation of Silver Nanoparticles. *Adv. Mater.* **2016**, *28*, 3712–3717. [\[CrossRef\]](#)
20. Muflikhun, M.A.; Syahril, M.; Mamba'udin, A.; Santos, G.N.C. A novel of hybrid laminates additively manufactured via material extrusion–vat photopolymerization. *J. Eng. Res.* **2023**, *11*, 100146. [\[CrossRef\]](#)
21. Yunus, D.E.; Sohrabi, S.; He, R.; Shi, W.; Liu, Y. Acoustic patterning for 3D embedded electrically conductive wire in stereolithography. *J. Micromech. Microeng.* **2017**, *27*, 045016. [\[CrossRef\]](#)
22. ISO 21920-2:2021; Geometrical product specifications (GPS) — Surface texture: Profile, Edition 1. ISO: Geneva, Switzerland, 2021; pp. 1–78.
23. ASTM\_D2240-15; Standard Test Method for Rubber Property—Durometer Hardness in ASTM D2240. ASTM: West Conshohocken, PA, USA, 2021; p. 13.
24. ASTM\_D638; Standard Test Method for Tensile Properties of Plastic. ASTM: West Conshohocken, PA, USA, 2022; p. 17.
25. Ganguly, S.; Chakraborty, S. Sedimentation of nanoparticles in nanoscale colloidal suspensions. *Phys. Lett. A* **2011**, *375*, 2394–2399. [\[CrossRef\]](#)
26. Mazzoli, A.; Moriconi, G. Particle size, size distribution and morphological evaluation of glass fiber reinforced plastic (GRP) industrial by-product. *Micron* **2014**, *67*, 169–178. [\[CrossRef\]](#)
27. Chen, T.-H.; Wang, I.-H.; Lee, Y.-R.; Hsieh, T.-H. Mechanical property of polymer composites reinforced with nanomaterials. *Polym. Polym. Compos.* **2021**, *29*, 696–704. [\[CrossRef\]](#)

28. Deng, W.; Xie, D.; Liu, F.; Zhao, J.; Shen, L.; Tian, Z. DLP-based 3D printing for automated precision manufacturing. *Mob. Inf. Syst.* **2022**, *2022*, 2272699. [[CrossRef](#)]
29. Hanon, M.M.; Ghaly, A.; Zsidai, L.; Szakál, Z.; Szabó, I.; Kátai, L. Investigations of the mechanical properties of DLP 3D printed graphene/resin composites. *Acta Polytech. Hung.* **2021**, *18*, 143–161. [[CrossRef](#)]
30. Vrochari, A.D.; Petropoulou, A.; Chronopoulos, V.; Polydorou, O.; Massey, W.; Hellwig, E. Evaluation of surface roughness of ceramic and resin composite material used for conservative indirect restorations, after repolishing by intraoral means. *J. Prosthodont.* **2017**, *26*, 296–301. [[CrossRef](#)]
31. Brinckmann, S.A.; Young, J.C.; Fertig, R.S.; Frick, C.P. Effect of print direction on mechanical properties of 3D printed polymer-derived ceramics and their precursors. *Mater. Lett. X* **2023**, *17*, 100179. [[CrossRef](#)]

**Disclaimer/Publisher’s Note:** The statements, opinions and data contained in all publications are solely those of the individual author(s) and contributor(s) and not of MDPI and/or the editor(s). MDPI and/or the editor(s) disclaim responsibility for any injury to people or property resulting from any ideas, methods, instructions or products referred to in the content.